Determination of Mechanical Stress Distribution in *Drosophila* Wing Discs Using Photoelasticity

Ulrike Nienhaus[1,2,3], Tinri Aegerter-Wilmsen[2] and Christof M. Aegerter[1,3]

1 Fachbereich Physik, Universität Konstanz, Universitätstrasse 10, Fach 688, 78457 Konstanz, Germany
2 Institute for Molecular Biology, Universität Zürich, Winterthurerstr. 190, 8057 Zürich, Switzerland
3 Physik-Institut, Universität Zürich, Winterthurerstr. 190, 8057 Zürich, Switzerland

Morphogenesis, the process by which all complex biological structures are formed, is driven by an intricate interplay between genes, growth, as well as intra- and intercellular forces. While the expression of different genes changes the mechanical properties and shapes of cells, growth exerts forces in response to which tissues, organs and more complex structures are shaped. This is exemplified by a number of recent findings for instance in meristem formation in Arabidopsis and tracheal tube formation in Drosophila. However, growth not only generates forces, mechanical forces can also have an effect on growth rates, as is seen in mammalian tissues or bone growth. In fact, mechanical forces can influence the expression levels of patterning genes, allowing control of morphogenesis via mechanical feedback. In order to study the connections between mechanical stress, growth control and morphogenesis, information about the distribution of stress in a tissue is invaluable. Here, we applied stress-birefringence to the wing imaginal disc of *Drosophila melanogaster*, a commonly used model system for organ growth and patterning, in order to assess the stress distribution present in this tissue. For this purpose, stress-related differences in retardance are measured using a custom-built optical set-up. Applying this method, we found that the stresses are inhomogeneously distributed in the wing disc, with maximum compression in the centre of the wing pouch. This compression increases with wing disc size, showing that mechanical forces vary with the age of the tissue. These results are discussed in light of recent models proposing mechanical regulation of wing disc growth.

Introduction

As was recognized by D'Arcy Thompson as early as the beginning of the 20th century, mechanical forces play a fundamental role during morphogenesis [Thompson, 1917]. However, the interplay between growth, mechanical forces and morphogenesis is much more intricate than he assumed. Expression levels of genes following a developmental programme determine the makeup and thus the mechanical properties of cells, thereby enabling them to exert the mechanical forces needed to collectively form spatial structures [Caussinus et al., 2008],[Oster et al., 1983]. These mechanical forces have in turn been shown to regulate gene expression and growth [Hamant et al., 2008],[Ingber, 2006],[Farge, 2003],[Kahn et al., 2009]. This enables the control of growth and patterning via feedback loops involving mechanical forces present in tissues, whereby non-uniform growth could relate back to itself via the development of mechanical stresses [Shraiman, 2005]. This raises the experimental question of assessing the mechanical stresses in developing tissues or growing organs in order to correlate the stresses present with morphological changes and growth control. So far this has only been done indirectly, either by disturbing the tissues using laser ablation and studying the ensuing relaxations [Hamant et al., 2008],[Caussinus et al., 2008] or by quantifying the strains present in the tissue by investigating the shape of the cells [Gorfinkiel et al., 2009].

A commonly studied model system for both growth and patterning is the wing imaginal disc of *Drosophila melanogaster*. A major morphogen and growth regulator in the wing disc is Decapentaplegic (Dpp), which is produced along the antero-posterior boundary and forms a gradient [Burke & Basler, 1996],[Lecuit et al., 1996],[Entchev et al., 2000],[Teleman & Cohen, 2000]. However, paradoxically, growth is uniform in the presence of this growth factor gradient [Milan et al., 1996], but becomes non-uniform when Dpp is expressed uniformly. In fact, in the latter case, growth rates are increased laterally and decreased medially [Rogulja & Irvine, 2005],[Schwank et al., 2008]. In light of the results in other organisms and the difficulties of purely morphogen-based approaches, models involving growth regulation via mechanical forces have recently been proposed for the wing disc [Shraiman, 2005],[Hufnagel et al., 2007],[Aegerter-Wilmsen et al., 2007].

Here, we employed photoelasticity on the tissue of the wing disc itself to determine the distribution of stress and its change during disc growth. The application of a mechanical stress to birefringent molecules leads to their orientation and stretching, subsequently resulting in a measurable change in birefringence, which is proportional to the applied stress. This change in birefringence corresponds to a change in the retardance of the light passing through the tissue [Majmudar & Behringer, 2005]. We measured this retardance using a sensitive optical setup and hence studied the spatial distribution of stresses in the wing imaginal disc. Furthermore, in order to ascertain that a photoelastic response was measured as opposed to merely a change in material density or thickness, we relieved stress by incisions and applied stress by stretching. This lead to a corresponding change in retardance, thus showing that birefringence can indeed be used to measure stresses in biological tissues.

In the case of wing discs, we found that there is an inhomogeneous distribution of mechanical stress with high compression in the centre of the disc. This compression increases with increasing disc size, showing that stress increases during growth and could thus play a part as regulators of growth. These findings are compared in more detail to recent models of growth regulation via mechanical forces, with which they are in good agreement. Finally, we observed that compression is also present in the centres of other types of imaginal discs, offering the possibility of a common size regulatory mechanism.

Results and Discussion

The spatial distribution of the retardance in a third instar wild-type wing disc is shown in Fig. 1a. The colourmap describes the magnitude of the retardance relative to that of insect Ringer's solution (IRS) of the same thickness. As can be seen in Fig. 1a, as well as Figs. 3 a-c below, the distribution of retardance in a wild type wing disc has a characteristic pattern. There is a circular region of higher birefringence in the area of the wing pouch with a distinct maximum in the centre, while the values in the rest of the wing disc are nearly constant.

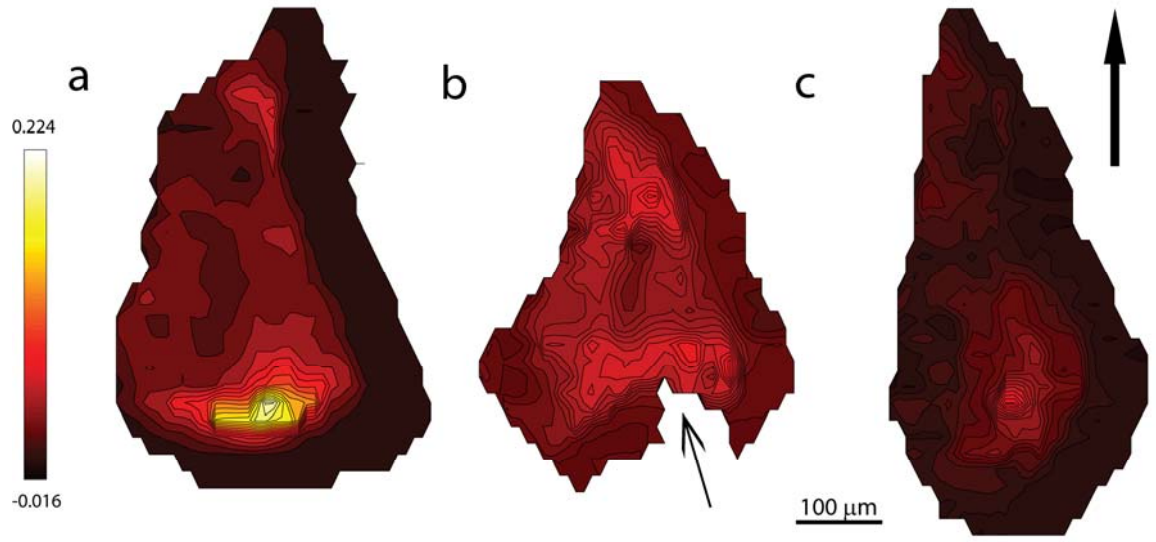

Figure 1. a) Distribution of retardance in a normal, late stage third instar wing disc. The retardance is highest in the centre of the wing pouch and the direction of the main stress can be seen from the orientation of the increased retardance relative to the incoming polarization (see supplementary figure). b) When a wing disc is cut, to relieve mechanical stresses, the retardance distribution changes accordingly. Here, the cut is indicated by an arrow. c) Direct mechanical stimulation by stretching the disc in the direction of the arrow also leads to a release of compression in the centre of the wing pouch. The disc shown here was of comparable size (width and length) as that in a) before stretching. The qualitative changes shown in b) and c) are observed in all stimulated wing discs (n=6 for cut, n=4 for stretched discs).

As discussed in the methods section, such a retardance distribution is expected in the presence of a mechanical stress, owing to stress-birefringence. Due to the presence of morphogen gradients as well as differential cell packing, the disc is not homogeneous and alternative sources of birefringence need to be controlled for. In particular, variations in thickness, density distributions of birefringent molecules, and the orientation of structures along the polarization direction could give rise to a similar distribution in retardance. Variations in thickness are unlikely, since confocal microscopy has shown that wing imaginal discs are of nearly constant thickness with a variation of roughly 10% [Gibson & Perrimon, 2005], such that in wing imaginal discs, retardance is also a direct measure of birefringence. Note that for the retardance, the whole of the imaginal disc has to be taken into account, i.e. the basal as well as the peripodial membrane. In order to further check for the different possible sources of birefringence we carried out several control experiments. Density gradients of birefringent molecules or variations in thickness should not show a definite orientation, such that the signal should be independent of the incoming polarization. For this reason, we measured the birefringence pattern for three different incoming polarizations, along the DV boundary, along the AP boundary as well as at an angle of 30 degrees to the DV boundary. The results are shown in Fig. 2 and indicate that the inhomogeneity in the wing pouch follows the orientation of the illuminating polarization, thus indicating that there is a definite orientation to the birefringence and no concentration gradient or thickness difference. This orientation and hence the principle stress difference follows the incoming polarization. Moreover, the levels of measured peak retardance are similar for discs comparable in size. This implies that the birefringence in the wing pouch is oriented roughly radially with a maximum in the centre. From a comparison of Fig 2a,c with Fig. 2b, it can be argued that the signal along the DV and AP axes is somewhat stronger thus indicating deviations

from radial symmetry. These differences could however also be due to the use of different wing discs in these measurements. In our current setup, it is however impossible to use only one disc due to the length of the scanning time for one image - similar uncertainties would arise because of the scanning time if one and the same disc were used in the experiment.

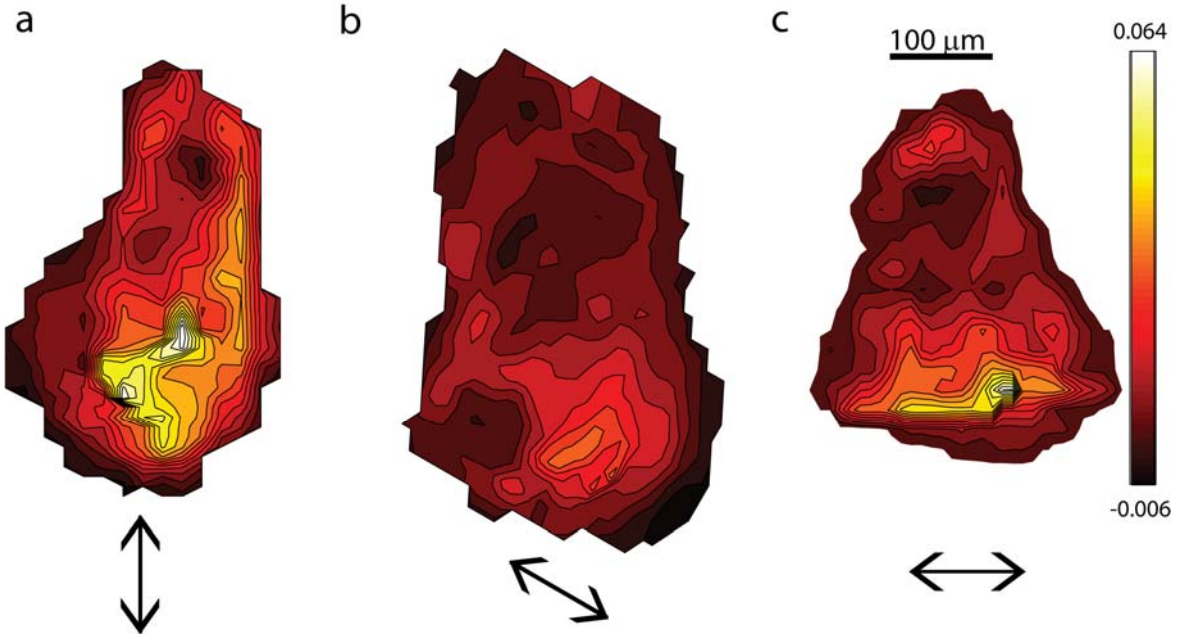

Figure 2: Retardance distribution with different incoming polarization directions. The polarization is indicated by the respective arrows below the figures. It can be seen that the inhomogeneities in retardance follow the orientation of the polarization, which implies that the difference in refractive index and thus the difference in the principle stress components does so as well. This implies that concentration differences of the material do not give rise to a birefringence distribution. Furthermore, the mostly horizontal features seen in the rest of the paper, which were obtained for horizontal incoming polarization, translate into a mainly radial stress distribution in the wing pouch.

Thus we have shown that concentration differences of any kind do not give rise to the inhomogeneous distribution in retardance, but different orientations of the optical axes of the tissue could still lead to similar results. To check for this, we incised the disc in the pouch region where birefringence is highest. This is expected to relieve mechanical stress and should therefore lead to a decrease in compression and hence retardance in the centre. Indeed, as can be seen in Fig. 1b, the peak in birefringence decreased greatly. The exact change in retardance depends on the location of the cut relative to the stress distribution but in all cases a decreased peak birefringence relative to that of a disc of comparable size is found (see figure 4, as well as supplementary figure S1). A student t-test comparing the peak retardances of the cut and uncut discs of the same size shows that the decrease in retardance is significant with a p-value of 0.03. This also shows that an inherent orientation of the tissue does not give rise to the signal, but rather that it is stress-related, as would be expected from stress-birefringence. Nevertheless, since measuring the birefringence of a disc takes more than an hour, we cannot formally exclude effects of wound-healing, resulting for example from the formation of actin cables [Wood et al., 2002]. However it is highly unlikely that such effects would lead to a decrease in retardance.

Finally, to confirm the interpretation of high and low birefringence values as compression and stretching, we also stretched wing discs lengthwise, in the direction of the arrow in Fig. 1c. This resulted in a decrease of the peak birefringence value, confirming that the high birefringence values indeed represent compression, a result which was found for all stretched discs studied, see Fig. 4. The open symbols represent experiments on the same disc before and after manipulation, which are possible for smaller discs because of the scanning time. A paired t-test of the experiments on the same discs gives a highly significant p-value of 0.002. The reduction in birefringence by more than a factor of two in response to an applied strain of ~30% again rules out the possibility that inhomogeneities in density could give rise to the observed distribution of birefringence. A change in density corresponding to such a strain would be much smaller. Note also that the corresponding shortening of the disc perpendicular to the direction of the stretching will not give rise to an increased stress and hence photoelastic signal. Moreover, the stretching experiments allow an order of magnitude estimate of the stress, since a significant strain (~30%) relieves most of the stress, yielding a stress of the order of the tissue's Young's modulus. For typical embryonic tissues the modulus was determined to be of the order of 0.1 to 0.01 N/m [Foty, 1996]. A quantitative measurement for the wing disc would need the application of a calibrated force.

Given that the birefringence maps can be regarded as maps of mechanical stress, it is interesting to study their development over time as the disc grows. Since discs could not be cultured for sufficiently long times or imaged in-vivo, this had to be done by investigating different discs at various stages of the third instar which varied strongly in size. We thereby used the widths of the discs as a measure of their age and found (see Fig. 3) that the compression in the centre increases greatly with age. We tested this correlation quantitatively by calculating the Spearman's rank of the data, which results in a value of 0.57, corresponding to a clearly significant correlation (p-value 0.008) given 23 different measurements of wing disc birefringence, i.e. 21 degrees of freedom for the correlation calculation.

Both the inhomogeneous stress distribution with the maximum compression in the centre as well as the increase of this compression with the age of the disc are in good agreement with recent predictions by two models of growth control via mechanical forces [Hufnagel et al., 2007],[Aegerter-Wilmsen et al., 2007]. These models are able to account for many observations, including uniform growth, and both propose that compression in the centre of the wing pouch eventually leads to the termination of disc growth. However, the two models differ fundamentally in the mechanisms by which the stresses are built up. In the model of Hufnagel et al., maximum growth rates depend on the local Dpp concentration. The Dpp gradient is assumed to be fixed, implying that growth rates decrease at the edge of the disc as the disc grows. This leads to increased stretching of this region and increased compression of the centre [Hufnagel et al., 2007]. The model of Aegerter-Wilmsen et al., in contrast, posits a stimulating effect of stretching on growth, even in the absence of Dpp, and a scaled Dpp gradient. In this model, compression increases due to the increasing width of the stretched region. When growth is terminated, the

level of stretching at the periphery of the disc is equal to a threshold value of stretching above which growth is induced. In smaller discs, this peripheral stretching can exceed the threshold, but it cannot be lower [Aegerter-Wilmsen et al., 2007]. Thus, with age, the peripheral stretching in [Aegerter-Wilmsen et al., 2007] is constant or decreasing, whereas [Hufnagel et al., 2007] predicts increasing stretching.

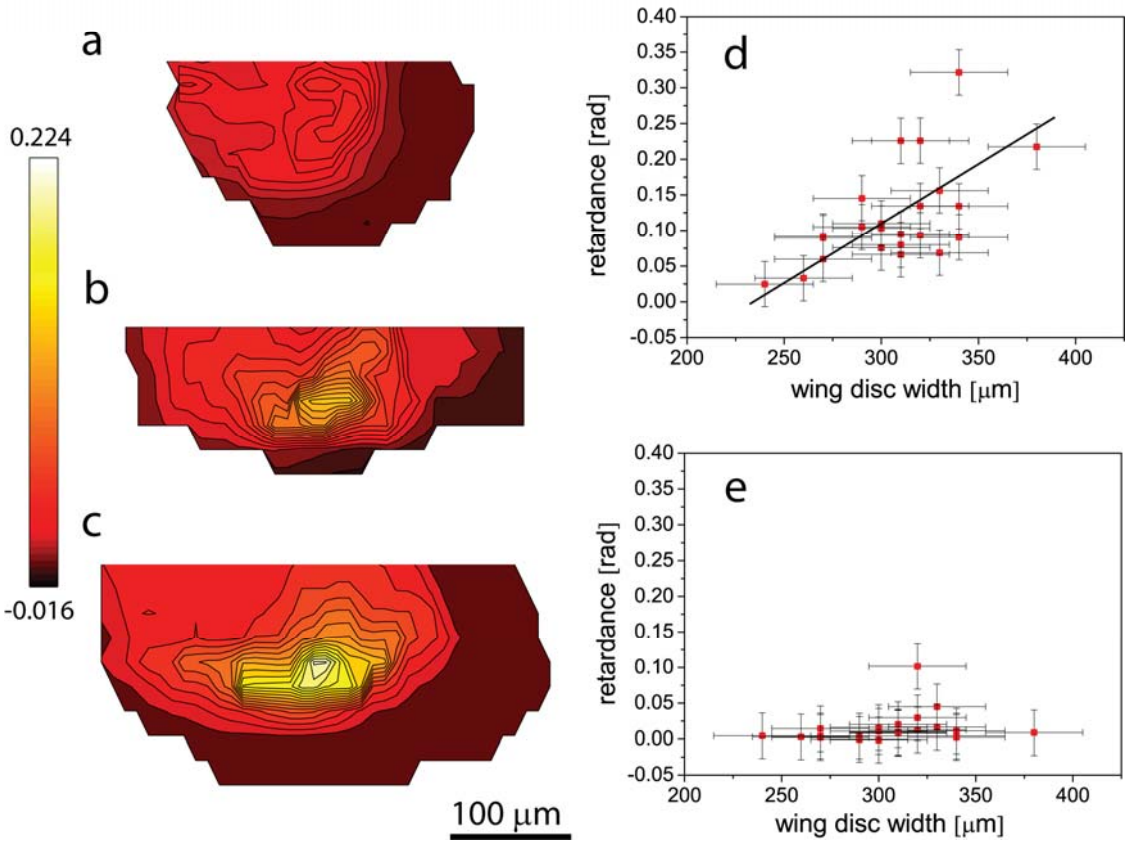

Figure 3: a-c) The retardance distribution in the wing pouch region at different stages of the 3rd instar larvae. As can be seen, with increasing size (age) compressive stress as indicated by retardance grows in the centre of the wing pouch. d) The measured peak retardance as a function of disc width. As predicted by the mechanical feedback models, the stress in the centre of the pouch increases with size. This is indicated by the straight line, which is meant as a guide to the eye. e) The size dependence of the retardance in the periphery. This is constant with size, in agreement with the model of Aegerter-Wilmsen et al. The error bars in d) and e) denote the uncertainties in the birefringence of a wing disc (vertically, due to e.g. drifts in the birefringence setup) as well as its horizontal size given by the step size of the scanning optical setup.

These predictions were tested experimentally via stress-birefringence, the result of which is shown in Fig. 3e, where we show the dependence of the retardance at the boundary on disc size. As can be seen, the retardance does not change with age, which indicates that stretching remains nearly constant during the growth of the wing disc, in agreement with [Aegerter-Wilmsen et al., 2007]. Again, we performed a Spearman's rank analysis, which yields a non significant correlation (p-value of 0.09).

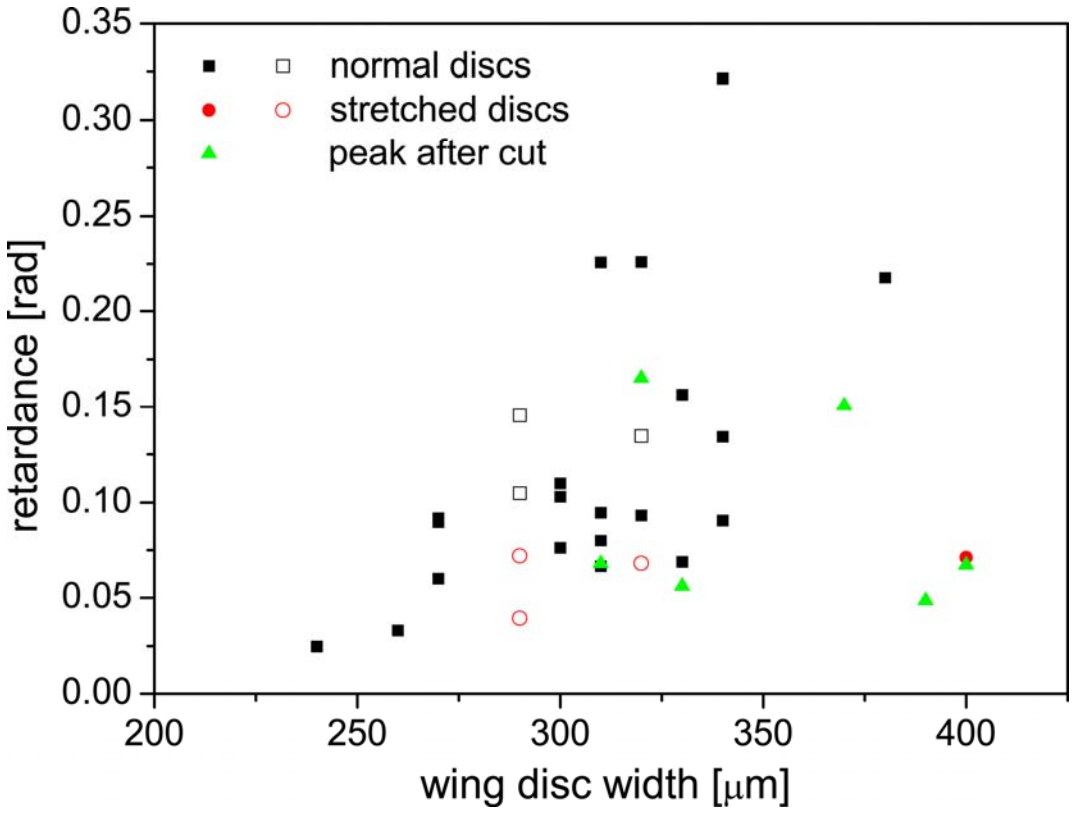

Figure 4: Peak retardance values for differently treated discs. Black squares correspond to normal wild type wing discs, whereas red dots correspond to stretched discs. The open symbols at intermediate size correspond to discs that have been measured before and after stretching. As can be seen, stretching greatly decreases the peak retardance by roughly 0.1 rad in all three cases shown here. A paired t-test gives a p-value of 0.002 for the significance of this decrease. Green triangles correspond to cut wing discs, where again the cut usually relieves stress, but depending on the position of the cut relative to the main stress, a peak can still be present, see also Fig. S1. Again we have tested the significance of this decrease using a t-test, yielding a significant p-value of 0.03.

Since there is a mechanical stress gradient present in wild-type discs which could cause uniform growth in combination with the Dpp gradient [Hufnagel et al., 2007],[Aegerter-Wilmsen et al., 2007] it would be interesting to see whether such a mechanical stress gradient is also present in discs with uniform Dpp signalling, where growth is non-uniform. For this purpose, we measured the stress distribution in discs ubiquitously expressing an activated form of the Dpp receptor Tkv. As is shown in Fig. 5a, the retardance pattern looks similar to the one observed for wild-type discs, except for the fact that the region of highest retardance seems to be somewhat larger. As in wild-type discs, the maximum peak intensity increases with disc width (supplementary figure S2) indicating that Tkv-QD discs also show a mechanical stress gradient.

Moreover, growth in different imaginal discs could lead to similar stress distributions and growth control mechanisms. We tested this premise experimentally by measuring the retardance maps of leg and eye-antennal discs. As is shown in Figs. 5b and c, these discs also show compression in the centre, indicating that size control may be achieved in a similar way in different discs.

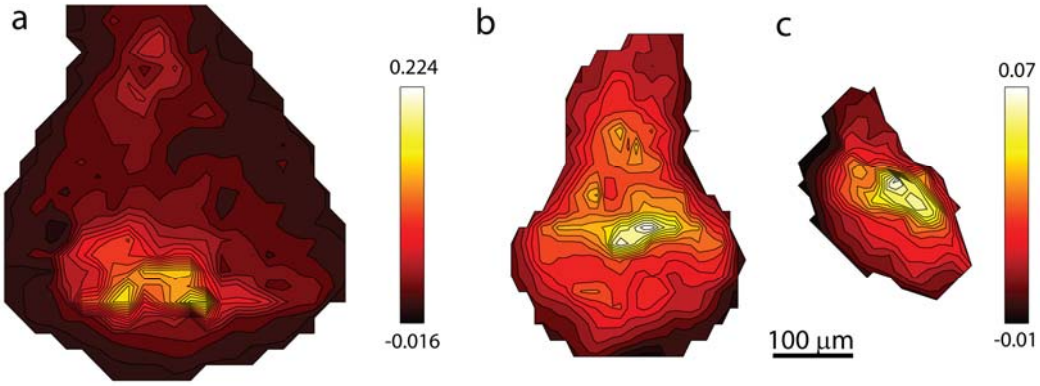

Figure 5: a) The retardance distribution in a wing disc with constitutive Dpp signaling. The stresses are distributed over a wider area than in the wild type situation. b) Retardance distribution in an eye-antennal imaginal disc. Here as well, a peak in retardance can be seen in the centre, which indicates that mechanical feedback could be a general mechanism of growth control. c) Retardance distribution in a leg disc. Similarly, a clear maximum in retardance can be seen as was the case in the wing and eye discs. Note that the colourmaps in b) and c) are different from that in a).

In conclusion, we have presented a method with which to measure mechanical stresses in biological tissues by birefringence measurements via photoelasticity. We have concentrated on the imaginal discs of *Drosophila*, which have revealed a stress distribution where compression builds up in the centre of the disc at the tissue level, in support of different recently proposed mechanical models [Hufnagel et al., 2007],[Aegerter-Wilmsen et al., 2007]. Thus the presence of a temporally variable stress-gradient can be used as a method of growth control in the wing disc. Comparing the different models, the constant level of stretching found in the peripheral regions of the disc favours [Aegerter-Wilmsen et al., 2007], although further experiments will be needed in order to test the assumptions underlying the models. Such experiments should ideally be done in a system capable of faster measurements of birefringence at higher resolution. This is in principle possible by using a modulated polarization setup on a standard microscope, which limits the resolution and speed to those of the microscope and the polarization modulation [Shribak & Oldenbourg, 2003],[Wijngaarden, 2004]. Moreover, it will be interesting to combine the observed stress pattern with the strains present in the tissue and study whether its mechanical properties play a role in the tissue deformations during metamorphosis. In this context it will be essential to repeat the stretching experiments above using calibrated forces, such that a map of the elastic properties can be obtained.

We also showed that there is a mechanical stress gradient present in discs with constitutive Dpp signalling. This stress gradient could contribute to differences in growth rates in these discs. It has also been proposed that decreased growth rates in the centre of these discs are caused by the disappearance of Dpp concentration differences in the centre [Rogulja & Irvine, 2005]. Indeed Dpp affects signalling by the

growth mediating hippo pathway [Rogulja et al., 2008] and hippo signalling differences induce growth [Oh & Irvine, 2008],[Willecke et al., 2008]. There is, however, also evidence against the hypothesis that Dpp concentration differences are necessary to induce growth [Schwank et al., 2008]. Further experiments are needed to explain the observed growth rate pattern and dissect the roles of Dpp, hippo signalling and mechanical stresses.

We found that the centres of the leg and eye-antennal discs are compressed as well. According to the mechanical growth models, net growth factor activity is highest in the centre. For the wing disc this could be achieved for example if both Wingless (Wg) and Dpp are required for growth [Couso et al., 1994], [Neumann & Cohen, 1996], [Diaz-Benjumea & Cohen, 1995], [Ng et al., 1996], [Giraldez & Cohen, 2003], even though the role of Wg is not yet completely clear [Johnston & Edgar, 1998], [Johnston & Sanders, 2003]. Alternatively, Notch induced signalling could be involved as well [Diaz-Benjumea & Cohen, 1995], [Giraldez & Cohen, 2003], [de Celis & Garcia-Bellido, 1994]. In the leg disc, Wg and Dpp have expression patterns that are distinct from those in the wing disc, but the combined concentration is still highest in the centre and both proteins are necessary to induce growth [Campbell et al., 1993],[Serrano & O'Farrell, 1997]. In the eye-antennal disc, the situation is more complicated since it is gradually subdivided into distinct organ domains and because of the presence of the morphogenetic furrow, which affects proliferation. However, in the centre there seems to be increased growth factor activity, since the growth factor eyegone (eyg) is expressed in the central region of eye discs in second instar discs and eyg itself can also induce unpaired (upd), which can increase proliferation over a distance [Cho & Choi, 1998],[Jang et al., 2003],[Tsai & Sun, 2004],[Chao et al., 2004]. Upstream regulators of eyg include wingless and notch. However, expression patterns of these genes show differences with those of the other discs (reviewed in [Dominguez & Casares, 2005]). It will be interesting to see whether the different imaginal discs indeed have similar size control mechanisms at the conceptional level, whereas they may differ in how the mechanisms are implemented.

Experimental procedures

Flies and Dissection

In most of the data below, wild type flies kept at room temperature were used. In order to induce uniform expression of UAS-tkvQ235D [Nellen et al., 1996], C765-Gal4 [Nellen et al., 1996] was used as a driver line. Third instar larvae were dissected in insect Ringer's solution (IRS) (7.5g NaCl, 0.35g KCl, 0.21g $CaCl_2$ made up with 1l of distilled water).

Sample Preparation

After dissection of a wing imaginal disc from a larva in one of the various stages of the third instar, a sample was prepared for measurement in a non-birefringent sample holder prepared as follows. First, a ring of tape was affixed to a quartz glass disc. A drop of poly-L-lysine (PLL) was placed inside this ring and the excess PLL

removed after about 30s, upon which a drop of IRS was placed inside the ring. In the next step, the wing disc was added to the sample cell and was attracted to the glass by the PLL. Finally, an identical glass disc was placed on top of the first.

The incisions into the wing discs, used to test the relaxation of stresses, were made using the tip of a syringe. Wing discs were stretched by attaching the tip of the wing disc to a surface using PLL and then pulling on the trachea at the notal end of the disc with a pair of micro forceps. The stretched discs were then attached to the surface using PLL.

Principles of Photoelasticity

Birefringent materials are anisotropic in that different axes of the material have different refractive indices, n_e along the extraordinary axis and n_o along the ordinary optical axis. Light, which is polarized in a given direction at an angle to these axes, has different amplitudes of the electromagnetic waves in the ordinary and extraordinary directions respectively. Due to the different refractive index, these components have different speeds along the optical axes in the birefringent material. This difference in speed of the different polarization states leads to a phase difference between the polarization components. This phase difference, the retardance δ, is directly proportional to the difference in the refractive indices of the ordinary and extraordinary axis, i.e. $\delta = 2\pi h\,(n_e - n_o)/\lambda$, where λ is the wavelength of the incident light and h is the material thickness. Thus if the two components are added behind the material, the overall polarization state is changed in proportion to the retardance. If a stress is now applied to a certain direction of such a birefringent material, the changes in the refractive indices in response to that stress will be different in the ordinary and extraordinary axes. This means that as a function of stress, the retardance of the sample changes in the direction of the applied stress. The situation is summarised in Fig. 6 and described by the fundamental relation of stress birefringence, which connects the components of the stress along the optical axes with the retardance, i.e. $\sigma_1 - \sigma_2 = c\ h\ (n_e - n_o)$, where c is the photoelastic constant describing the magnitude of the stress-birefringence. Thus by measuring the retardance of a sample in different incoming polarization states, the principle stresses and their directions can be determined. Due to the fact that its polarization is progressively changed during the light's passage through the birefringent material, this technique works best in transparent, flat tissue of constant thickness. These criteria are reasonably well fulfilled in wing imaginal discs as discussed above. An observed retardance is given by the product of the birefringence and the thickness of the wing disc at each point. Therefore, in order to determine the stress inhomogeneities in the material, patterns in the retardance have to be attributed either to birefringence or thickness. As noted above, the photoelastic change in retardance and therefore in birefringence is proportional to the applied stress, where the direction of the stress determines the fast optical axis [Frocht, 1948],[Frocht, 1941]. In contrast to other origins of birefringence, such as those implied by concentration differences of the material, an inherent orientation is implied in photoelasticity. This effect can be tested by measuring the birefringence with different incoming polarization states. Given a definite direction, the birefringence will follow the

orientation of the polarization. A more in depth account of photoelasticity is given in the textbooks of Frocht [Frocht, 1948],[Frocht, 1941].

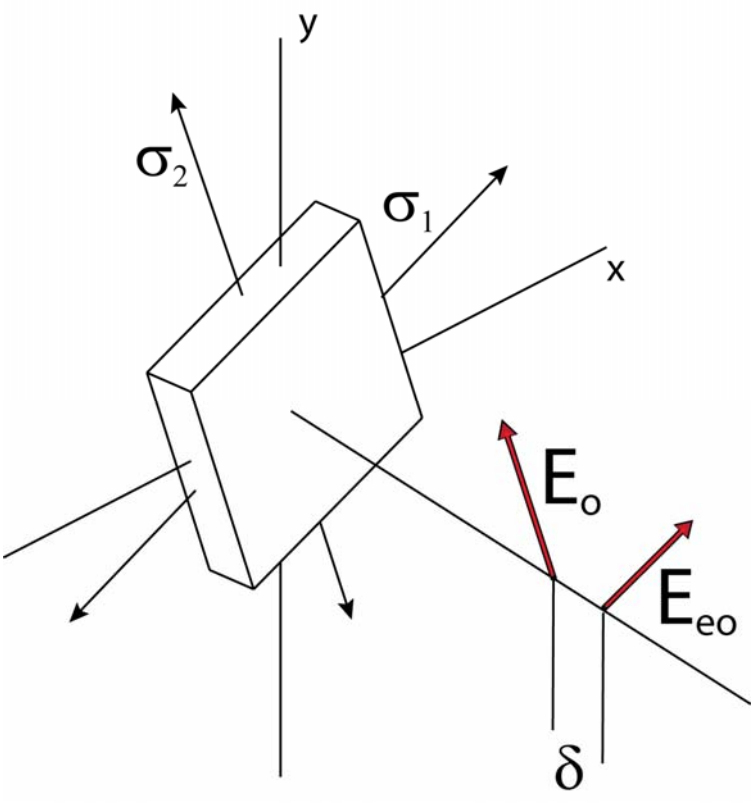

Figure 6: Schematic of an idealised photoelasticity experiment. Light enters a birefringent material from the left in a given polarization state. Due to the different refractive indices of the material along the different axes (o and eo), there is a phase shift in the light that passes through a sample. This phase shift is the retardance due to the birefringence of the material. When a stress is applied along one these directions, its refractive index changes leading to a corresponding change in the measured retardance. When the stress is at an angle to the optical axes, only a projection of the stress is turned into a retardance signal.

Experimental Set-up

The optical set-up used ([Maret et al., 1975], Fig. 7) is capable of measuring differences in retardance of 0.002 rad. It consists of a crossed polarizer/analyzer pair between which are located a babinet-soleil compensator (BSC), a Pockels cell, an objective for focusing the illumination, the sample holder and a photoelastic modulator (PEM). A photodiode is located behind the analyzer. As a light source, an argon-ion laser with a wavelength of 514.5nm is used.

The electrical set-up included a lock-in amplifier (LIA), which receives a signal from the photodiode and a reference signal from the PEM, followed by an integrator, a multimeter and a high voltage source. The basic principle of the setup consists in compensating the retardance of the sample in combination with the BSC using the Pockels cell. As long as the two induced phase shifts are not opposite and equal, meaning that there is no total phase shift, the LIA receives a signal from the photodiode which is in phase with the reference signal from the PEM. The LIA continuously applies a voltage proportional to the received signal to the integrator.

After integration, the integrator applies the resulting voltage to the high voltage source controlling the Pockels cell. This voltage value is also displayed on the multimeter.

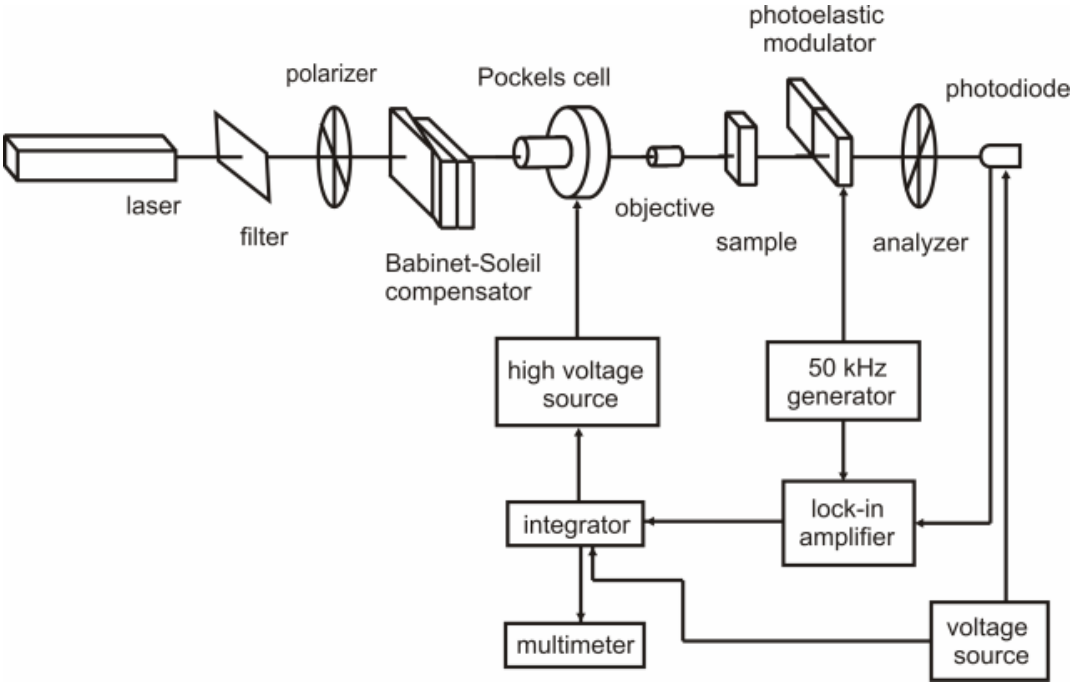

Figure 7: Schematic of the optical set-up. The focus of the objective is scanned across the sample for spatial resolution. See text for details.

The setup quickly regulates the phase shift induced by the Pockels cell to be equal and opposite to that induced by the sample and BSC. This phase shift can then be calculated from the voltage applied to the Pockels cell after calibration of the set-up using only the BSC as a sample. The phase shift induced by the BSC during the experiments was constant and could therefore be subtracted to obtain the phase shift induced by the sample.

A birefringence map of the sample was created by scanning it across the focus of the illuminating laser using translation stages. The retardance was measured in about 1,000 points in increments of 20 microns in the vertical direction and 10 microns in the horizontal direction given by the translation stages. By this method, we are able to determine the retardance, or phase shift in different points of a wing disc, thus producing a two dimensional retardance map.

Acknowledgements

We would like to thank T. Schluck for useful discussions as well as K. Basler and E. Hafen for comments on the manuscript and G. Schwank (Basler lab), Institute of Molecular Biology University of Zurich, for providing the tkvQD mutant flies. This work was partially supported by SystemsX.ch within the framework of the WingX RTD and the Roche research foundation.

References

[Aegerter-Wilmsen et al., 2007] Aegerter-Wilmsen, T., Aegerter, C. M., Hafen, E. & Basler, K. (2007). Mechanisms of Development 124, 318–326.

[Burke & Basler, 1996] Burke, R. & Basler, K. (1996). Development 122, 2261–2269.

[Campbell et al., 1993] Campbell, G., Weaver, T. & Tomlinson, A. (1993). Cell 74, 1113–1123.

[Caussinus et al., 2008] Caussinus, E., Colombelli, J. & Affolter, M. (2008). Curr. Biol. 18, 1727–1734.

[Chao et al., 2004] Chao, J.-L., Tsai, Y.-C., Chiu, S.-J. & Sun, Y. H. (2004). Development 131, 3839–3847.

[Cho & Choi, 1998] Cho, K.-O. & Choi, K.-W. (1998). Nature 396, 272–276.

[Couso et al., 1994] Couso, J., Bishop, S. & Martinez Arias, A. (1994). Development 120, 620–636.

[de Celis & Garcia-Bellido, 1994] de Celis, J. & Garcia-Bellido, A. (1994). Mech. Dev. 46, 109–122.

[Diaz-Benjumea & Cohen, 1995] Diaz-Benjumea, F. & Cohen, S. (1995). Development 121, 4215–4225.

[Dominguez & Casares, 2005] Dominguez, M. & Casares, F. (2005). Developmental Dynamics 232, 673–684.

[Entchev et al., 2000] Entchev, E., Schwabedissen, A. & Gonzalez-Gaitan, M. (2000). Cell 103, 981–991.

[Farge, 2003] Farge, E. (2003). Current Biology 13, 1365–1377.

[Foty, 1996] Foty, R.A.; Pfleger, C.M., Forgacs, G. & Steinberg, M.S. (1996). Development 122, 1611.

[Frocht, 1941] Frocht, M. M. (1941). Photoelasticity, Volume 1.

[Frocht, 1948] Frocht, M. M. (1948). Photoelasticity, Volume 2.

[Gibson & Perrimon, 2005] Gibson, M. & Perrimon, N. (2005). Science 307, 1785–1789.

[Giraldez & Cohen, 2003] Giraldez, A. J. & Cohen, S. M. (2003). Development 130, 6533–6543.

[Gorfinkiel et al., 2009] Gorfinkiel, N., Blanchard, G., Adams, R. & Martinez Arias, A. (2009). Development 136, 1889–1898.

[Hamant et al., 2008] Hamant, O., Heisler, M. G., Jonsson, H., Krupinski, P., Uyttewaal, M., Bokov, P., Corson, F., Sahlin, P., Boudaoud, A., Meyerowitz, E. M., Couder, Y. & Traas, J. (2008). Science 322, 1650–1655.

[Hufnagel et al., 2007] Hufnagel, L., Teleman, A. A., Rouault, H., Cohen, S. M. & Shraiman, B. I. (2007). Proceedings of the National Academy of Sciences 104, 3835–3840.

[Ingber, 2006] Ingber, D. (2006). Intl. J. Dev. Biol. 50, 255–266.

[Jang et al., 2003] Jang, C., Chao, J., Jones, N., Yao, L., Bessarab, D., Kuo, Y., Jun, S., Desplan, C., Beckendorf, S. & Sun, Y. (2003). Development 130, 2939–2951.

[Johnston & Edgar, 1998] Johnston, L. A. & Edgar, B. A. (1998). Nature 394, 82–84.

[Johnston & Sanders, 2003] Johnston, L. A. & Sanders, A. L. (2003). Nat Cell Biol 5, 827–833.

[Kahn et al., 2009] Kahn, J., Shwartz, Y., Blitz, E., Krief, S., Sharir, A., Breitel, D.A., Rattenbach, R., Relaix, F., Maire, P., Rountree, R.B., Kingsley, D.M. & Zelzer, E. (2009). Developmental Cell, 16, 734 – 743.

[Lecuit et al., 1996] Lecuit, T., Brook, W. J., Ng, M., Calleja, M., Sun, H. & Cohen, S. M. (1996). Nature 381, 387–393.

[Majmudar & Behringer, 2005] Majmudar, T. S. & Behringer, R. P. (2005). Nature 435, 1079–1082.

[Maret et al., 1975] Maret, G., Schickfus, M. v., Mayer, A. & Dransfeld, K. (1975). Phys. Rev. Lett. 35, 397–400.

[Milan et al., 1996] Milan, M., Campuzano, S. & Garcia-Bellido, A. (1996). Proceedings of the National Academy of Sciences of the United States of America 93, 640–645.

[Nellen et al., 1996] Nellen, D., Burke, R., Struhl, G. & Basler, K. (1996).

[Neumann & Cohen, 1996] Neumann, C. & Cohen, S. (1996). Development 122, 3477–3485.

[Ng et al., 1996] Ng, M., Diaz-Benjumea, F. J., Vincent, J.-P., Wu, J. & Cohen, S. M. (1996). Nature 381, 316–318.

[Oh & Irvine, 2008] Oh, H. & Irvine, K. D. (2008). Development 135, 1081–1088.

[Oster et al., 1983] Oster, G. F., Murray, J. D. & Harris, A. K. (1983). J. Embryol. exp. Morph. 78, 83–125.

[Rogulja & Irvine, 2005] Rogulja, D. & Irvine, K. D. (2005). Cell 123, 449 – 461.

[Rogulja et al., 2008] Rogulja, D., Rauskolb, C. & Irvine, K. D. (2008). Developmental Cell 15, 309 – 321.

[Schwank et al., 2008] Schwank, G., Restrepo, S. & Basler, K. (2008). Development 135, 4003–4013.

[Serrano & O'Farrell, 1997] Serrano, N. & O'Farrell, P. (1997). Curr. Biol. 7, R186–R195.

[Shraiman, 2005] Shraiman, B. I. (2005). Proceedings of the National Academy of Sciences of the United States of America 102, 3318–3323.

[Shribak & Oldenbourg, 2003] Shribak, M. & Oldenbourg, R. (2003). App. Optics 42, 3009–3017.

[Teleman & Cohen, 2000] Teleman, A. & Cohen, S. (2000). Cell 103, 971–980.

[Thompson, 1917] Thompson, D. W. (1917). On Growth and Form.

[Tsai & Sun, 2004] Tsai, Y.-C. & Sun, Y. H. (2004). genesis 39, 141–153.

[Wijngaarden, 2004] Wijngaarden, R.J.; Welling, M.S., Aegerter, C.M. & Heek, K. (2004). MOI of pattern formation in the vortex landscape 142, 61.

[Willecke et al., 2008] Willecke, M., Hamaratoglu, F., Sansores-Garcia, L., Tao, C. & Halder, G. (2008). Proceedings of the National Academy of Sciences 105, 14897–14902.

[Wood et al., 2002] Wood, W., Jacinto, A., Grose, R., Woolner, S., Gale, J., Wilson, C. & Martin, P. (2002). Nat Cell Biol 4, 907–912.

Supplementary Figures

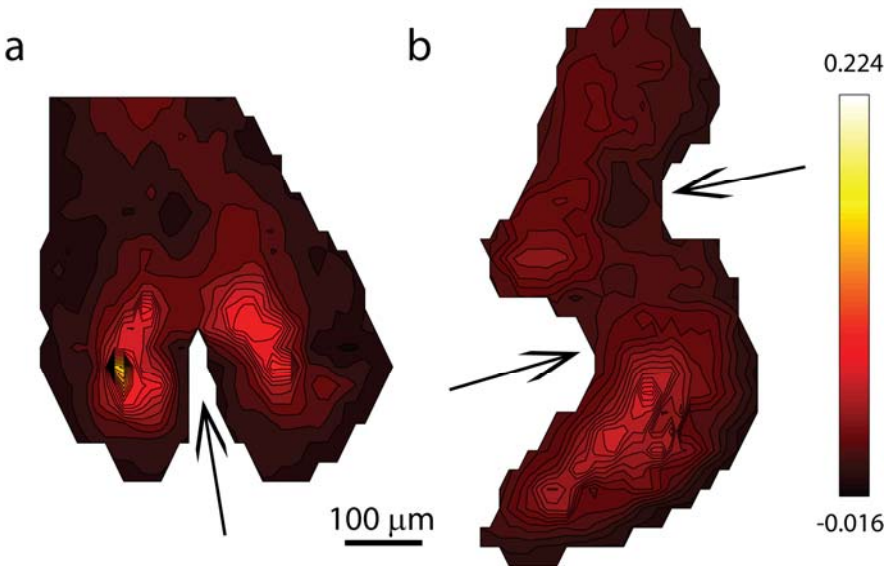

Figure S1: Retardance distributions in wing discs after cuts through different regions of the pouch. In all cases, the peak retardance is reduced with respect to a disc of comparable size, but depending on the exact location of the cut, some stress remains inside the wing disc after cutting. The colourmap is the same as in figure 2 of the main paper.

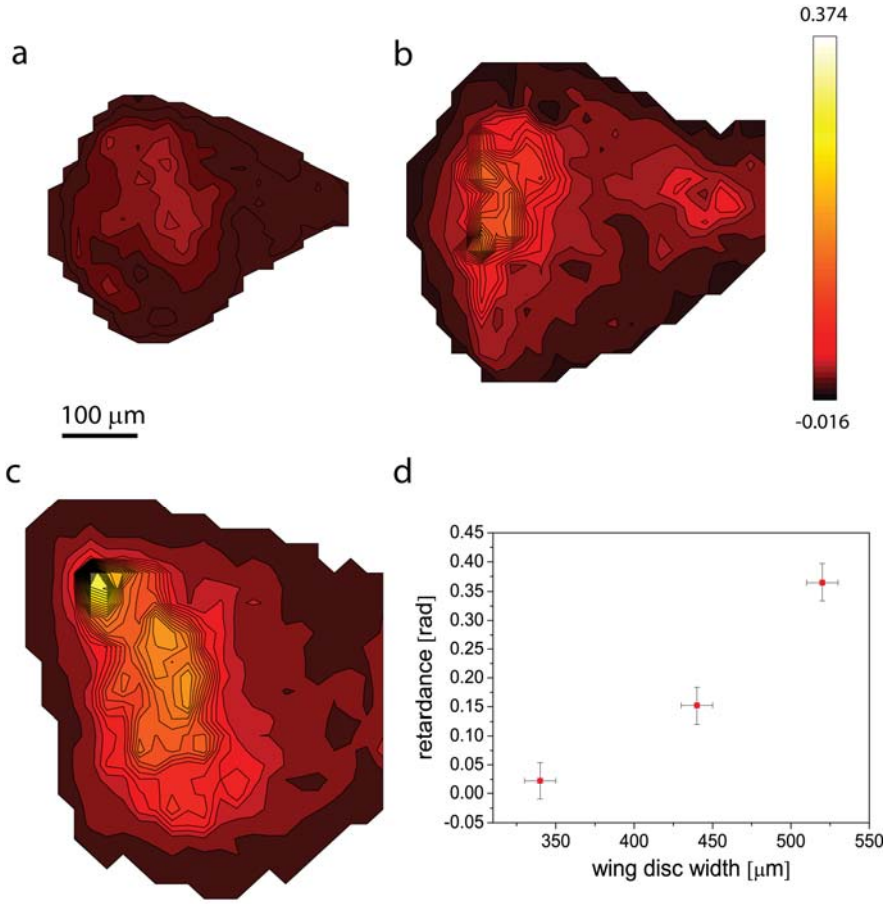

Figure S2: a-c) Wing discs with constitutive Dpp signalling at different stages of the third instar. As was the case in the wild type flies, the stress in the centre of the wing pouch increases with age. d) Dependence of the peak retardance with disc width showing the increase of compression with age.